

REVIEW

Three-dimensional analysis of mandibular growth and tooth eruption

S. Krarup,^{1,2,3} T. A. Darvann,² P. Larsen,² J. L. Marsh⁴ and S. Kreiborg^{1,2,3,5}

¹Department of Pediatric Dentistry and Clinical Genetics, School of Dentistry, Faculty of Health Sciences, University of Copenhagen, Copenhagen, Denmark

²3D-Laboratory, School of Dentistry, Faculty of Health Sciences, University of Copenhagen, Copenhagen University Hospital, and The Technical University of Denmark

³Department of Oral and Maxillofacial Surgery, and ⁵The Copenhagen Craniofacial Unit, Copenhagen University Hospital, Copenhagen, Denmark

⁴Pediatric Plastic Surgery, Cleft Lip/Palate & Craniofacial Deformities Center, St John's Mercy Medical Center, St Louis, MO, USA

Abstract

Normal and abnormal jaw growth and tooth eruption are topics of great importance for several dental and medical disciplines. Thus far, clinical studies on these topics have used two-dimensional (2D) radiographic techniques. The purpose of the present study was to analyse normal mandibular growth and tooth eruption in three dimensions based on computer tomography (CT) scans, extending the principles of mandibular growth analysis proposed by Björk in 1969 from two to three dimensions. As longitudinal CT data from normal children are not available (for ethical reasons), CT data from children with Apert syndrome were employed, because it has been shown that the mandible in Apert syndrome is unaffected by the malformation, and these children often have several craniofacial CT scans performed during childhood for planning of cranial and midface surgery and for follow-up after surgery. A total of 49 datasets from ten children with Apert syndrome were available for study. The number of datasets from each individual ranged from three to seven. The first CT scan in each of the ten series was carried out before 1 year of age, and the ages for the 49 scans ranged from 1 week to 14.5 years. The mandible and the teeth were segmented and iso-surfaces generated. Landmarks were placed on the surface of the mandible, along the mandibular canals, the inner contour of the cortical plate at the lower border of the symphysis menti, and on the teeth. Superimposition of the mandibles in the longitudinal series was performed using the symphysis menti and the mandibular canals as suggested by Björk. The study supported the findings of stability of the symphysis menti and the mandibular canals as seen in profile view previously reported by Björk & Skieller in 1983. However, the mandibular canals were, actually, relocated laterally during growth. Furthermore, the position of tooth buds remained relatively stable inside the jaw until root formation started. Eruption paths of canines and premolars were vertical, whereas molars erupted in a lingual direction. The 3D method would seem to offer new insight into jaw growth and tooth eruption, but further studies are needed.

Key words CT; development; facial growth; jaw; three dimensions.

Introduction

Normal and abnormal facial growth and tooth eruption are topics of great importance for several dental

disciplines, such as pedodontics, orthodontics, and oral and maxillofacial surgery. All clinical studies have, thus far, been carried out using two-dimensional (2D) roentgencephalometric techniques (e.g. Björk, 1968; Björk & Kuroda, 1968; Björk & Skieller, 1972, 1983).

The techniques of roentgencephalometry were originally developed 70 years ago by orthodontic researchers (Hofrath, 1931; Broadbent, 1931), searching for a method that would make possible the longitudinal study of growth of the jaws in children through standardized,

Correspondence

Professor Sven Kreiborg, Department of Pediatric Dentistry and Clinical Genetics, School of Dentistry, Faculty of Health Sciences, University of Copenhagen, Nørre Alle 20, 2200 Copenhagen N, Denmark.

E: sven@odont.ku.dk

Accepted for publication 1 July 2005

reproducible skull X-rays with known magnification and minimal distortion. Broadbent's technique has gained worldwide acceptance within the field of orthodontics as an indispensable clinical and research tool. Perspectives in the application of roentgencephalometry to clinical orthodontics and to the study of craniofacial anomalies have been extensively reviewed by Ricketts (1981) and Kreiborg (1985), respectively. Although the basic technique of Broadbent's cephalometric method has remained almost unaltered over the years, several significant technical improvements have been made (Björk, 1951, 1968; Pruzansky & Lis, 1958; Kreiborg et al. 1977; Solow & Kreiborg, 1988), which again have led to development of refined analytical methods (Björk, 1955, 1968; Walker, 1967; Kreiborg, 1981; Hermann et al. 2001). One of the most significant analytical improvements in roentgencephalometry included the use of metallic implants in the jaws (Björk, 1955, 1968). This method made it possible to distinguish between displacement and surface remodelling of the individual jaw and to study tooth eruption in longitudinal studies of facial growth (Björk, 1968; Björk & Skieller, 1972, 1983) (see Fig. 1). This method of analysis

of jaw growth has been a major step forward in our understanding of normal growth of the face. Based on their extensive implant studies, Björk (1969) and Björk & Skieller (1983) suggested that superimposition of cephalometric films or drawings in longitudinal series of individual children can be carried out on stable natural, anatomical reference structures without the use of metallic implants. For the mandible these structures are: (1) the anterior contour of the chin; (2) the inner contour of the cortical plate at the lower border of the symphysis menti; (3) any distinct trabecular structure in the symphysis menti; (4) the contour of the mandibular canal; and (5) the lower contour of mineralized tooth germs before root development begins (Fig. 2). This superimposition technique today represents a paradigm.

One of the most severe problems in roentgencephalometry is, however, to control head position during exposure. Ideally, the head should be positioned according to the Frankfurt horizontal and the plane of symmetry at every examination including both the lateral and the frontal projections (Fig. 3). However, in conventional cephalometry control of head positioning is often flawed by error (see Fig. 3), leading to analytical

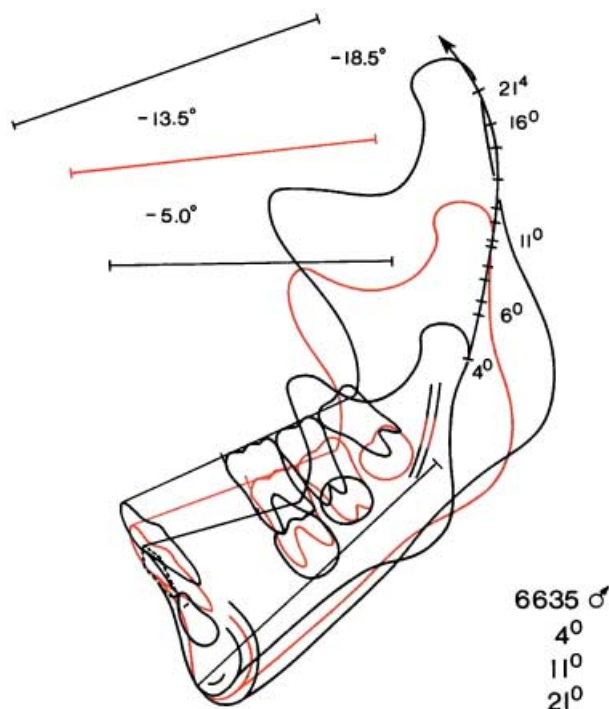


Fig. 1 Two-dimensional mandibular growth analysis from 4 to 21 years of age in a normal individual, based on cephalometric radiographs in the lateral projection and superimposed on metallic implants inserted into the jaw. Note the surface remodelling and the eruption of the teeth. (Modified from Björk & Skieller, 1983.)



Fig. 2 Anatomical reference structures: (1) the anterior contour of the chin; (2) the inner contour of the cortical plate at the lower border of the symphysis menti; (3) any distinct trabecular structure in the symphysis menti; (4) the contour of the mandibular canal; (5) the lower contour of mineralized tooth germs before root development begins. (Modified from Björk & Skieller, 1983.)

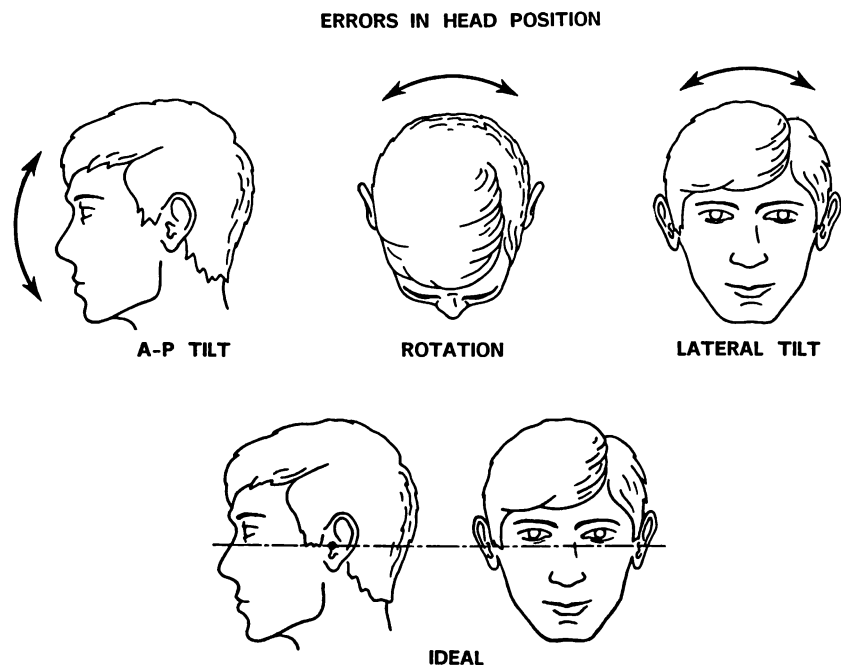


Fig. 3 Ideal head position in the cephalometer (below), and potential errors in head position (above) which will result in various types of distortion in the radiographs.

problems when studying jaw growth and tooth eruption. A few cephalometric units for research purposes have, however, attempted to solve these problems by, in addition to ear-rods, employing light-crosses projected on the face and an image intensifier (Björk, 1968; Kreiborg et al. 1977; Solow & Kreiborg, 1988). Another serious shortcoming of roentgencephalometric analyses is that throughout they are limited to two dimensions. With the introduction of high-resolution computer tomography (CT) scans to the craniofacial region, it became possible to make 3D reconstructions of the craniofacial skeleton (Marsh & Vannier, 1983). These techniques have led to numerous qualitative as well as quantitative analyses of craniofacial morphology, primarily in subjects with various types of congenital craniofacial anomalies (Abbott et al. 1990, 2000; Marsh et al. 1991; Kreiborg et al. 1993; Vannier et al. 1994; Lo et al. 1996; Vannier & Marsh, 1996; Cavalcanti & Vannier, 1998; Zumpano et al. 1999; Kane et al. 2000). However, only very few attempts have been made to analyse craniofacial growth in three dimensions (Bro-Nielsen et al. 1997; Andresen et al. 2000; Kreiborg et al. 2001; Hilger et al. 2003), although one of the advantages of the technique over conventional cephalometric techniques is that errors in head positioning during exposure can be corrected for by uprighting the 3D model in the computer after the scan has been performed. The purpose of the present study was to analyse

normal mandibular growth and tooth eruption in three dimensions, extending the principles of mandibular superimposition on 'stable, natural, anatomical reference structures' (Björk, 1969; Björk & Skieller, 1983) from two to three dimensions, thereby testing the paradigm related to the stability of these structures.

Materials and methods

Sample

Ten children with Apert syndrome were included in the study, five males and five females. Apert syndrome is characterized by craniostenosis, midface hypoplasia, and symmetric syndactyly of the hands and feet, minimally involving digits 2, 3 and 4. The inheritance is autosomal dominant with a male-to-female ratio of 1 : 1 and with most cases representing new mutations (Cohen, 2000). Kreiborg et al. (1999) reported a cephalometric study of craniofacial morphology in patients with Apert syndrome. Marked differences were found in nearly all craniofacial regions except the mandible, which was of normal size and shape. Tooth development is normal, whereas tooth eruption is somewhat delayed, especially in the maxilla, because of crowding (Kreiborg & Cohen, 1992; Kaloust et al. 1997). The ten cases with Apert syndrome included in the present study had been followed and treated by The Cleft

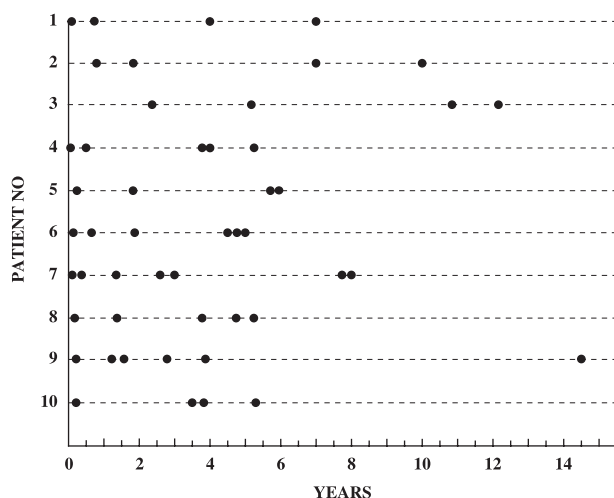


Fig. 4 Ten patients with Apert syndrome. Indication of age at time of CT scans.

Palate and Craniofacial Deformities Institute at St Louis Children's Hospital or by The Copenhagen Craniofacial Unit (CCFU) at Copenhagen University Hospital. All children were Caucasian, and all had received some kind of calvarial and/or maxillary surgery. However, no mandibular surgery had been carried out in any of the cases. All patients had had craniofacial CT scans performed in connection with diagnosis, treatment planning and postoperative follow-up. Only patients for whom CT scans had been carried out at least three times over time were included in the study. The ages at which CT scans was performed in the individual patients are given in Fig. 4. The ages ranged from 1 week to 14.5 years, and the number of scans per patient ranged from three to seven. A total of 49 CT datasets were obtained from the ten patients for clinical purposes, and after clinical use these datasets were made available for the 3D-Laboratory for the present study.

Acquisition of CT data

All scans were performed in Siemens CT scanners. The data were obtained over the period 1984–2000. Twenty-nine datasets were obtained in a Siemens DR2 scanner with a slice thickness of 2.0 mm and 256 × 256 matrix, and 20 scans were performed using a Siemens Somatom Plus 4 scanner with a slice thickness of 2.0 mm and 512 × 512 matrix. All scans were otherwise carried out using the same protocol. All data were transferred from the scanners to a powerful graphics computer (Silicon Graphics Onyx2).

Data processing

Data processing consisted of three consecutive steps, pre-processing, landmark definition and digitization, and registration.

Pre-processing

Once the data had been transferred to the Silicon Graphics Onyx2 computer, data conversion was carried out, converting ACR NEMA-files and DICOM-files to Analyze™ format. Following the conversion, the CT scans were checked for motion artefacts and the correct left-right orientation was ascertained.

Landmark definition and digitization

Registration of structures and growth analysis were based on employment of landmarks.

Two types of landmarks were used, anatomical landmarks and pseudo-landmarks (Dryden & Mardia, 1998). The mandible and the teeth (permanent canines, premolars, molars) were segmented using a combination of manual segmentation and threshold selection. Iso-surfaces were generated and rendered using the software package Mvox™ (Anamedic, 1999). Application of this method has previously been described by Bro-Nielsen et al. (1996) and Kreiborg et al. (1996a,b). All landmarks were placed using one of three methods. (1) Interactive landmarks in three orthogonal image slice views, with interactive intensity (window/level) adjustment. This method was applied when registration was made on the mandibular canal and the symphysis menti. (2) Interactive landmarks on under-segmented structures represented as polygonal 3D structures, iso-intensity surfaces with automatic correction. This method was applied when registration was made on the teeth. Landmarks were placed on 3D iso-intensity surfaces, as this provided a more precise localization of landmarks than would have been possible using three 2D orthogonal image slice views. In order to separate the teeth from the jaw bone, a high threshold selection is necessary. This leads, however, to 'under-segmentation' of the teeth, thereby underestimating their true size. This error was adjusted for by an automatic correction of the landmark position. The corrected landmark position was chosen to be the first maximum of the intensity gradient in the cranial direction of the tooth, corresponding to the edge of the

tooth. The position and the direction of the long axis of the individual tooth was defined by landmarks or points calculated from landmarks. (3) Interactive landmarks on structures represented as polygonal 3D structures, iso-intensity surfaces. This method was applied to registration of the mandible. The threshold selected in rendering the mandible as a polygonal 3D structure was chosen to be that particular threshold in each CT scan where all soft tissue was seen to disappear.

A total of 28 skeletal and 84 dental landmarks were employed. Six of the skeletal landmarks were placed in the mid-sagittal plane, whereas 11 were identical for the right and left side ($n = 22$). All dental landmarks were bilateral. Some landmarks were not identifiable on all patients and some landmarks were only identifiable at certain ages. Definitions of the skeletal and dental landmarks are given in Tables 1 and 2, and are illustrated in Figs. 5 and 6, respectively. Digitization was carried out using the software package Mvox™. All landmarks were digitized directly on the 3D rendered iso-intensity surfaces, except for the mental foramina and the centres of the dental vacuoles, which were

digitized from the 2D slices. The mandibular canals were localized in as many slices as possible. The matrix was perpendicular, and sequential landmarks were digitized at the centre of the canal in each CT slice, using the software package Analyze™ (AnalyzeDirect, 1999). The inner contour of the cortical plate at the lower border of the symphysis menti was localized on one sagittal CT slice in the midline and sequential landmarks were digitized, using the software package Mvox™.

Registration

Registration of growth in a patient and comparison of growth within the sample were carried out using least-squares estimation (Press et al. 1992) of the best fit between 3D landmarks representing homologous points in pairs of landmark datasets. In those cases where anatomical landmarks could not be found, pseudo-landmarks along an anatomical structure were identified instead (for the mandibular canal and the symphysis menti). The registration problem was solved

Table 1 Skeletal landmarks on the mandible (see Fig. 5)

id	Infradentale. The most antero-superior point of the inferior alveolar process.
sm	Supramentale. The most posterior point on the anterior contour of the inferior alveolar process.
pg	Pogonion. The most anterior point on the symphysis menti.
pgn	Prognathion. The point on the symphysis menti furthest from condylion.
gn	Gnathion. The most inferior point on the symphysis menti.
sp	Sympathys posterior. The most posterior point on the posterior contour of the symphysis menti.
Agd	Antegonion dexter. The highest point in the antegonial notch on the right side.
mlpd	Mandibular line, posterior point dexter. The posterior tangent point of the ML on the right side.
Apd	Angulus posterior dexter. The inferior tangent point of the RL on the right side.
Cdid	Condylion inferior dexter. The most anterior point on the posterior contour of the mandibular ramus on the right side.
Cdd	Condylion dexter. The most supero-posterior point on the mandibular condyle on the right side.
Cldd	Condylion lateralis dexter. The most lateral point on the mandibular condyle on the right side.
cdmd	Condylion mesialis dexter. The most mesial point on the mandibular condyle on the right side.
Imd	Incisura mandibulae dexter. The deepest point on the mandibular incisure on the right side.
Pcd	Processus coronoideus dexter. The most superior point on the coronoid process on the right side.
Rad	Ramus anterior dexter. Deepest point on the anterior contour of the mandibular ramus on the right side.
Mfd	Mental foramen dexter. The entrance to the mental canal on the right side.
Ags	Antegonion sinister. The highest point in the antegonial notch on the left side.
Mlps	Mandibular line, posterior point sinister. The posterior tangent point of the ML on the left side.
Aps	Angulus posterior sinister. The inferior tangent point of the RL on the left side.
Cdis	Condylion inferior sinister. The most anterior point on the posterior contour of the mandibular ramus on the left side.
Cds	Condylion sinister. The most supero-posterior point on the mandibular condyle on the left side.
Cdls	Condylion lateralis sinister. The most lateral point on the mandibular condyle on the left side.
Cdms	Condylion mesialis sinister. The most mesial point on the mandibular condyle on the left side.
Ims	Incisura mandibulae sinister. The deepest point on the mandibular incisure on the left side.
Pcs	Processus coronoideus sinister. The most superior point on the coronoid process on the left side.
Ras	Ramus anterior sinister. Deepest point on the anterior contour of the mandibular ramus on the left side.
Mfs	Mental foramen sinister. The entrance to the mental canal on the left side.

ML, mandibular line. The tangent to the lower border of the mandible through gn. RL, ramus line. The tangent to the posterior border of the mandible.

Table 2 Dental landmarks* (Fig. 6)

M3mfs	The top of the mesio-facial cusp on the third mandibular molar on the left side.
M3cfs	The top of the centro-facial cusp on the third mandibular molar on the left side.
M3dfs	The top of the disto-facial cusp on the third mandibular molar on the left side.
M3mLs	The top of the mesio-lingual cusp on the third mandibular molar on the left side.
M3 dL	The top of the disto-lingual cusp on the third mandibular molar on the left side.
M3ts	The centre of the occlusal surface on the third mandibular molar on the left side.
M3bs	The centre of the bottom ¹ on the third mandibular molar on the left side.
M3vacs	The centre of the dental vacuole ² on the third mandibular molar on the left side.
M2(4) ³ mfs	The top of the mesio-facial cusp on the second molar on the left side.
M2(4)cfs	The top of the centro-facial cusp on the second mandibular molar on the left side.
M2(4)mls	The top of the mesio-lingual cusp on the second mandibular molar on the left side.
M2(4) dLs	The top of the disto-lingual cusp on the second mandibular molar on the left side.
M2(5) ⁴ mfs	The top of the mesio-facial cusp on the second molar on the left side.
M2(5)cfs	The top of the centro-facial cusp on the second mandibular molar on the left side.
M2(5)dfs	The top of the disto-facial cusp on the second mandibular molar on the left side.
M2(5)mls	The top of the mesio-lingual cusp on the second mandibular molar on the left side.
M2(5)dls	The top of the disto-lingual cusp on the second mandibular molar on the left side.
M2ts	The centre of the occlusal surface on the second mandibular molar on the left side.
M2bs	The centre of the bottom on the second mandibular molar on the left side.
M2vacs	The centre of the dental vacuole on the second mandibular molar on the left side.
M1mfs	The top of the mesio-facial cusp on the first mandibular molar on the left side.
M1cfs	The top of the centro-facial cusp on the first mandibular molar on the left side.
M1dfs	The top of the disto-facial cusp on the first mandibular molar on the left side.
M1mls	The top of the mesio-lingual cusp on the first mandibular molar on the left side.
M1dl	The top of the disto-lingual cusp on the first mandibular molar on the left side.
M1ts	The centre of the occlusal surface on the first mandibular molar on the left side.
M1bs	The centre of the bottom on the first mandibular molar on the left side.
M1vacs	The centre of the dental vacuole on the first mandibular molar on the left side.
P2fs	The top of the facial cusp on the second mandibular premolar on the left side.
P2ts	The centre of the upper surface ⁵ on the mineralized tissue of the second mandibular premolar on the left side.
P2(3)dls	The top of the disto-lingual cusp on the second mandibular premolar on the left side.
P2(3)mls	The top of the mesio-lingual cusp on the second mandibular premolar on the left side.
P2(2)ls	The top of the lingual cusp on the second mandibular premolar on the left side.
P2bs	The centre of the bottom ⁶ on the second mandibular premolar on the left side.
P1fs	The top of the facial cusp on the first mandibular premolar on the left side.
P1ts	The centre of the upper surface on the mineralized tissue of the first mandibular premolar on the left side.
P1(3)dls	The top of the disto-lingual cusp on the first mandibular premolar on the left side.
P1(3)mls	The top of the mesio-lingual cusp on the first mandibular premolar on the left side.
P1(2)ls	The top of the lingual cusp on the first mandibular premolar on the left side.
P1bs	The centre of the bottom on the first mandibular premolar on the left side.
Cfs	The top of the facial cusp on the mandibular canine on the left side.
Cbs	The centre of the bottom ⁷ on the mandibular canine on the left side.
M3mfd	The top of the mesio-facial cusp on the third mandibular molar on the right side.
M3cf	The top of the centro-facial cusp on the third mandibular molar on the right side.
M3dfd	The top of the disto-facial cusp on the third mandibular molar on the right side.
M3mld	The top of the mesio-lingual cusp on the third mandibular molar on the right side.
M3 dLd	The top of the disto-lingual cusp on the third mandibular molar on the right side.
M3td	The centre of the occlusal surface on the third mandibular molar on the right side.
M3bd	The centre of the bottom on the third mandibular molar on the right side.
M3vacd	The centre of the dental vacuole on the third mandibular molar on the right side.
M2(4)mfd	The top of the mesio-facial cusp on the second molar on the right side.
M2(4)cfd	The top of the centro-facial cusp on the second mandibular molar on the right side.
M2(4)mld	The top of the mesio-lingual cusp on the second mandibular molar on the right side.
M2(4) dLd	The top of the disto-lingual cusp on the second mandibular molar on the right side.
M2(5)mfd	The top of the mesio-facial cusp on the second molar on the right side.
M2(5)cfd	The top of the centro-facial cusp on the second mandibular molar on the right side.
M2(5)dfd	The top of the disto-facial cusp on the second mandibular molar on the right side.
M2(5)mld	The top of the mesio-lingual cusp on the second mandibular molar on the right side.
M2(5)dld	The top of the disto-lingual cusp on the second mandibular molar on the right side.
M2td	The centre of the occlusal surface on the second mandibular molar on the right side.

Table 2 Continued

M2bd	The centre of the bottom on the second mandibular molar on the right side.
M2vacd	The centre of the dental vacuole on the second mandibular molar on the right side.
M1mfd	The top of the mesio-facial cusp on the first mandibular molar on the right side.
M1cfd	The top of the centro-facial cusp on the first mandibular molar on the right side.
M1dfd	The top of the disto-facial cusp on the first mandibular molar on the right side.
M1mld	The top of the mesio-lingual cusp on the first mandibular molar on the right side.
M1dLd	The top of the disto-lingual cusp on the first mandibular molar on the right side.
M1td	The centre of the occlusal surface on the first mandibular molar on the right side.
M1bd	The centre of the bottom on the first mandibular molar on the right side.
M1vacd	The centre of the dental vacuole on the first mandibular molar on the right side.
P2fd	The top of the facial cusp on the second mandibular premolar on the right side.
P2td	The centre of the upper surface on the mineralized tissue of the second mandibular premolar on the right side.
P2(3)dld	The top of the disto-lingual cusp on the second mandibular premolar on the right side.
P2(3)mld	The top of the mesio-lingual cusp on the second mandibular premolar on the right side.
P2(2)ld	The top of the lingual cusp on the second mandibular premolar on the right side.
P2bd	The centre of the bottom on the second mandibular premolar on the right side.
P1fd	The top of the facial cusp on the first mandibular premolar on the right side.
P1td	The centre of the upper surface on the mineralized tissue of the first mandibular premolar on the right side.
P1(3)dld	The top of the disto-lingual cusp on the first mandibular premolar on the right side.
P1(3)mld	The top of the mesio-lingual cusp on the first mandibular premolar on the right side.
P1(2)ld	The top of the lingual cusp on the first mandibular premolar on the right side.
P1bd	The centre of the bottom on the first mandibular premolar on the right side.
Cfd	The top of the facial cusp on the mandibular canine on the right side.
Cbd	The centre of the bottom on the mandibular canine on the right side.

*Not all patients in the study had the same number of essential cusps on the same tooth type. A combination of the landmarks listed here includes all variations encountered.

¹Centre of the bottom: on molars, defined as the centre of the furcation or centre of the bottom of the crown if root development had not begun.

²Centre of the dental vacuole: defined as the centre of the vacuole in that particular transversal slice in which the dental vacuoles were seen to have the largest diameter.

³(4): four-cusp variant.

⁴(5): five-cusp variant.

⁵Centre of the upper surface: on premolars, defined as the centre of the upper surface on the mineralized tissue, if no cusps were identifiable due to low degree of crown mineralization.

⁶Centre of the bottom: on premolars, defined as the centre of the furcation, centre of the root cones or centre of the bottom of the crown if root development had not begun.

⁷Centre of the bottom: on canines, defined as the centre of the root cones or centre of the bottom of the crown if root development had not begun.

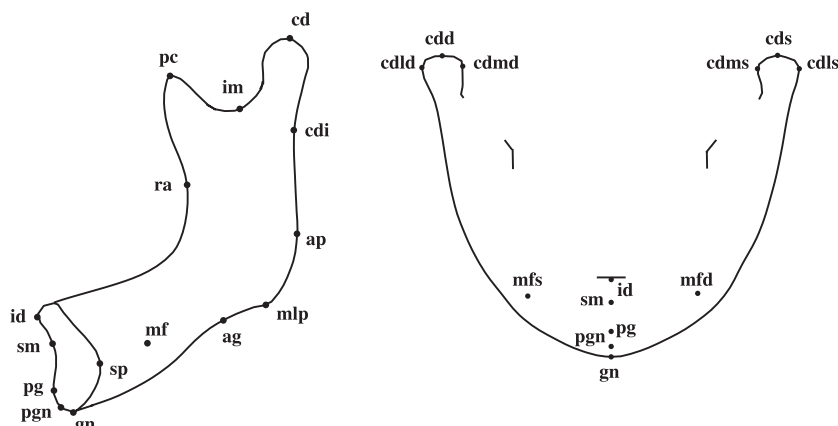


Fig. 5 Skeletal landmarks illustrated in the lateral and frontal aspects.

by use of the Iterative Closest Point Algorithm (Zhang, 1994), which iteratively employs the following two steps until convergence. (1) At every spatial point on the reference mandible, estimate an approximate homolo-

gous point on the structure to be registered by use of closest points. (2) Move the structure to be registered after estimating the best fit by use of the method of least squares (Press et al. 1992).

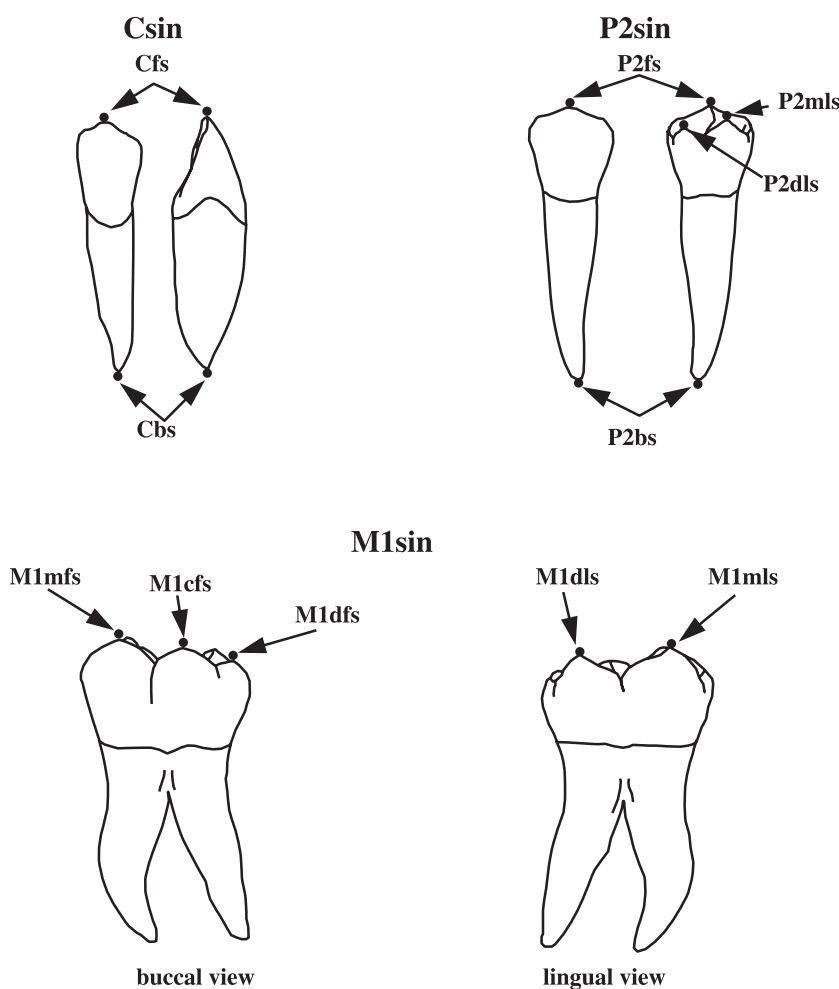


Fig. 6 Dental landmarks illustrated on a mandibular left canine, second left premolar and first left molar. The top and bottom landmarks on the molar are not shown. (Modified from Carlsen, 1987.)

Analysis

For growth measurements, morphology was represented by landmarks (Tables 1 and 2).

The growth of a specific anatomical structure in a patient was defined as the displacement vector from the coordinates of a landmark at examination 1 to the coordinates of the same landmark at examination 2.

Statistical methods

The error of the method for landmark localization and placement on mandible, teeth, vacuoles and mental foramina was determined using $s(i)$, encompassing both systematic and random error. $s(i)$ has been used by many orthodontic investigators and represents the mean square error (Dahlberg, 1940; Houston, 1983). $s(i)$ is defined as $\sqrt{(\sum d^2)/2N}$, where $d = x_1 - x_2$. x_1 and x_2 are

the coordinates of a landmark at the first and second digitization, respectively, and N is the number of paired measurements.

Spline curves were fitted to the sequential landmarks digitized along the mandibular canal and the inner cortical surface of the symphysis menti. The mandibular canals and the symphysis menti from the same scan were grouped. The difference between duplicate digitizations of the same grouping was determined using the Iterative Closest Point Algorithm. This routine was repeated until little or no change was observed. The error $s(i)$ between corresponding points was then calculated as $\sqrt{\frac{\sum d^2}{2N}}$, d = the mean distance between spline curve groupings derived from the first and second digitization. The numerical value of $s(i)$ will be similar to the numerical value of $s(i)$, calculated from d . The computation of variables and statistical data was carried out by use of IDL (Interactive Data Language, 1997).

Table 3 Calculated method errors (mm) for skeletal landmarks (Fig. 5). Right side and left side combined

Name	<i>n</i>	\bar{d}	$s(i)$	s	min	max
Id	46	0.541	0.463	0.373	0.076	2.276
Sm	43	0.428	0.357	0.272	0.120	1.249
Pg	43	0.599	0.571	0.549	0.112	2.837
Pgn	39	0.730	0.654	0.576	0.043	2.308
Gn	41	0.852	0.766	0.678	0.111	2.475
Sp	46	0.899	0.816	0.732	0.041	2.870
ag	91	0.742	0.673	0.599	0.008	3.381
mlp	90	0.596	0.503	0.390	0.051	2.161
ap	92	0.862	0.752	0.626	0.039	2.504
cdi	94	0.726	0.620	0.496	0.049	2.606
cd	94	0.663	0.593	0.516	0.040	2.452
im	94	0.485	0.444	0.402	0.030	2.062
pc	94	0.466	0.383	0.276	0.019	1.190
ra	94	0.807	0.696	0.565	0.055	2.759
cdl	92	0.475	0.400	0.310	0.051	1.484
cdm	92	0.756	0.623	0.455	0.041	2.450
Mf	80	0.860	0.701	0.498	0.098	2.320

Results

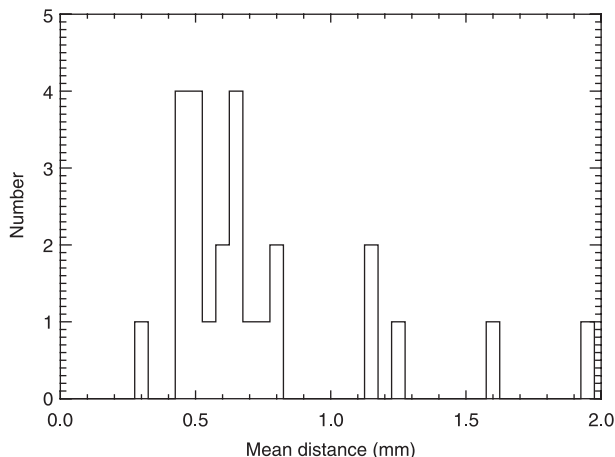
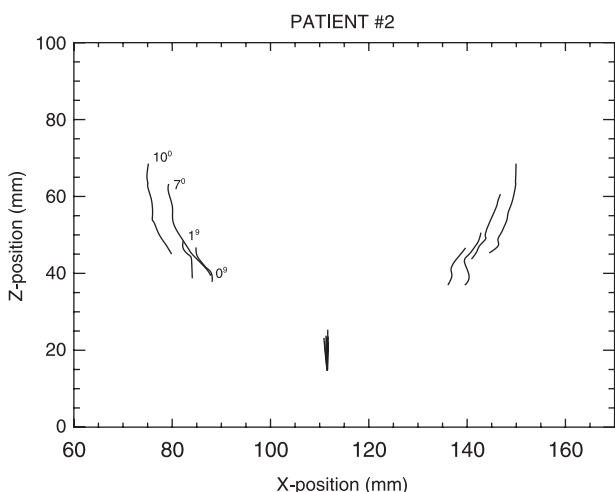
Error of the method

The error of the landmark digitization was determined by duplicate digitizations. The difference between the first and the second digitization ranged from 0.008 to 3.381 mm for the skeletal landmarks (Table 3) and from 0.030 to 2.423 mm for the dental landmarks (Table 4). [M3b, M2b, M1b, P2b, P1b and Cb excluded because bottom landmarks, used only for orientation, in some cases were placed in a different level, i.e. slice, than used in the first digitization.] The $s(i)$ values ranged from 0.357 to 0.816 mm and 0.271 to 0.770 mm, respectively.

The error of the pseudo-landmark digitization determined by duplicate digitizations is given in Table 5. The mean $s(i)$ value was 0.589 mm. The histogram distribution of the mean difference, \bar{d} , between the first and the second digitization is illustrated in Fig. 7. As can be seen from the figure, 20 of the 25 mean values (80%) were below 1 mm.

Mandibular growth

Mandibular growth was documented by superimposed computed plots (frontal and lateral views) of each of the ten patients. The superimpositions were performed using the symphysis menti and the mandibular canals

**Fig. 7** Histogram distribution of the mean difference, \bar{d} , between the first and the second digitization ($N = 25$).**Fig. 8** Patient no. 2. Frontal view. Superimposed plots showing the symphysis menti and the mandibular canals at four different ages (0, 1, 7 and 10 years), as indicated in the figure.

at each stage. Superimposed plots of one representative case are shown in Figs. 8 and 9.

The qualitative analysis of the plots revealed the following common features. (1) The symphysis menti showed an increase in antero-posterior width, primarily as a consequence of bone apposition posteriorly. (2) In lateral view, the curvature of the mandibular canals remained relatively stable over time, and the canals increased in length posteriorly. (3) In frontal view the mandibular canals revealed a lateral shift in all cases.

Inspecting the superimposed surface model (Fig. 10), it could be observed that the remodelling pattern had the following characteristics: (1) bone apposition at the condyle, coronoid process, alveolar process, posterior

Name	n	\bar{d}	s(i)	s	min	max
M3mf	2	–	–	–	–	–
M3cf	2	–	–	–	–	–
M3df	2	–	–	–	–	–
M3ml	2	–	–	–	–	–
M3dl	2	–	–	–	–	–
M3t	6	0.709	0.554	0.365	0.052	1.172
M2(4)mf	10	0.412	0.409	0.429	0.061	1.506
M2(4)cf	10	0.397	0.317	0.218	0.128	0.807
M2(4)ml	10	0.314	0.271	0.231	0.042	0.866
M2(4)dl	10	0.402	0.339	0.274	0.061	0.921
M2(5)mf	16	0.458	0.408	0.363	0.066	1.520
M2(5)cf	16	0.379	0.297	0.187	0.130	0.754
M2(5)df	16	0.482	0.490	0.514	0.073	2.021
M2(5)ml	16	0.512	0.442	0.371	0.191	1.674
M2(5)dl	16	0.523	0.474	0.432	0.059	1.448
M2t	32	0.554	0.454	0.329	0.123	1.334
M1(5)mf	68	0.448	0.444	0.444	0.062	2.131
M1(5)cf	68	0.365	0.347	0.330	0.043	1.824
M1(5)df	68	0.468	0.420	0.369	0.045	1.729
M1(5)ml	68	0.462	0.395	0.317	0.030	1.515
M1(5)dl	68	0.491	0.428	0.356	0.067	1.720
M1t	66	0.533	0.435	0.311	0.072	1.672
P2f	12	0.597	0.550	0.521	0.040	1.590
P2(3)ml	10	0.671	0.610	0.572	0.194	2.210
P2(3)dl	10	0.552	0.434	0.283	0.222	1.031
P2(2)l	2	–	–	–	–	–
P2t	8	0.585	0.474	0.350	0.201	1.142
P1f	14	0.496	0.421	0.343	0.058	1.461
P1(2)l	14	0.881	0.770	0.664	0.243	2.423
Pt	26	0.561	0.451	0.310	0.068	1.154
Cf	70	0.692	0.614	0.529	0.083	2.240
M3b*	6	0.590	0.459	0.297	0.130	0.943
M2b*	32	0.599	0.736	0.865	0.100	5.149
M1b*	66	0.577	0.618	0.661	0.088	5.076
P2b*	20	0.404	0.329	0.237	0.133	1.105
P1b*	40	0.405	0.333	0.243	0.103	1.196
Cb*	70	0.624	0.601	0.581	0.064	3.092
M3vac	6	0.753	0.711	0.729	0.245	2.089
M2vac	38	0.612	0.603	0.603	0.055	2.319
M1vac	42	0.602	0.632	0.668	0.079	2.372

*These points were excluded from the analysis as bottom landmarks, used only for orientation, in some cases were placed in a different level, i.e. slice, than used in the first digitization.

aspect of the ramus, and on the labial/buccal surface of the mandible; and (2) bone resorption at the anterior aspect of the ramus, underneath the gonion and on the lingual aspect of the body of the mandible, especially in the regions of the coronoid process, the ramus, and the condyle.

Tooth eruption

A qualitative analysis of the superimposed surface model with segmentation of the permanent teeth

Table 4 Calculated method errors (mm) for dental landmarks (Fig. 6). Right side and left side combined

Table 5 Calculated method errors (mm), for spline curve groupings. N = 25

	Mean Σd	Mean s(i)	s
Spline curve groupings	0.742	0.589	0.380

posterior to the incisors (Figs. 10–14) showed that the first and second molars erupted in a lingual direction whereas the canines and premolars seemed to erupt in an almost straight vertical direction seen in the

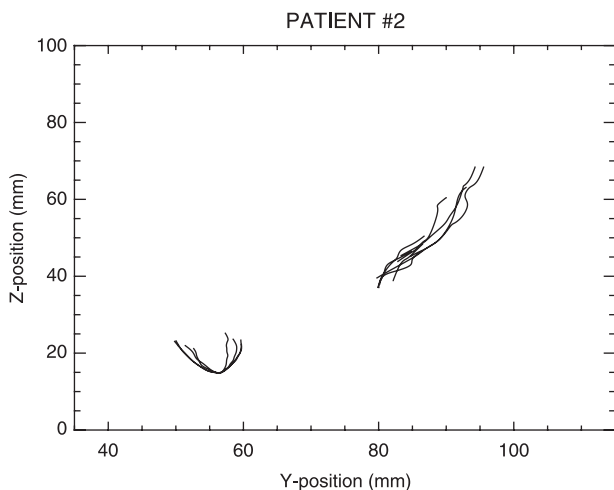


Fig. 9 Patient no. 2. Lateral view. Superimposed computed plots showing the symphysis menti and the mandibular canals at four different ages (0, 1, 7 and 10 years).

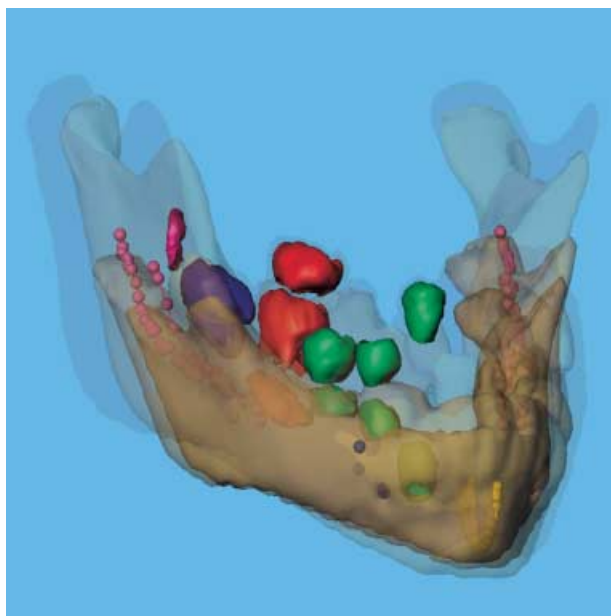


Fig. 10 Patient no. 2. Oblique view. Three-dimensional superimposition of transparent mandibles at four different ages (0, 1, 7 and 10 years). Mental foramina, and segmented teeth (posterior to the incisors) from four different ages (0, 1, 7 and 10 years) are aligned automatically on the symphysis menti and the mandibular canals. Only the teeth and the mental foramen on the right side are illustrated. Tooth colour code: purple = permanent third molar, blue = permanent second molar, red = permanent first molar, and green = permanent premolars and the permanent canine. The mental foramen = blue. The symphysis menti = yellow. The mandibular canals = pink.

frontal plane (Fig. 11). In addition, the study showed that teeth which have not started to develop the root remain relatively stable inside the jaw during that period.

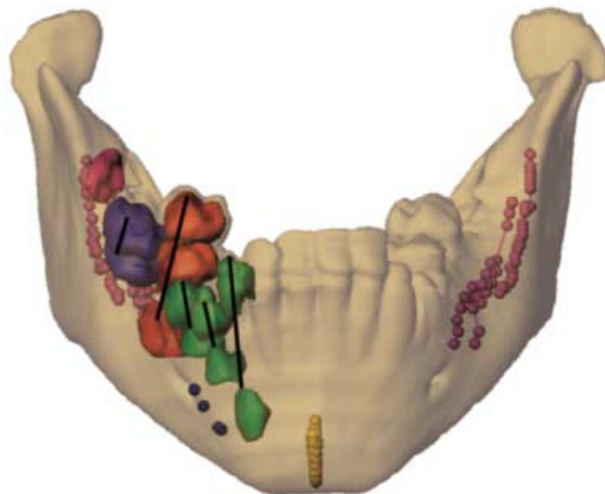


Fig. 11 Patient no. 2. Frontal view. Transparent mandible at age 10 years. Mental foramina, and segmented teeth (posterior to the incisors) from four different ages (0, 1, 7 and 10 years) are aligned automatically on the symphysis menti and the mandibular canals. Only the teeth and the mental foramen on the right side are illustrated. Lines indicate the eruption paths of the individual teeth. For colour coding see Fig. 10.

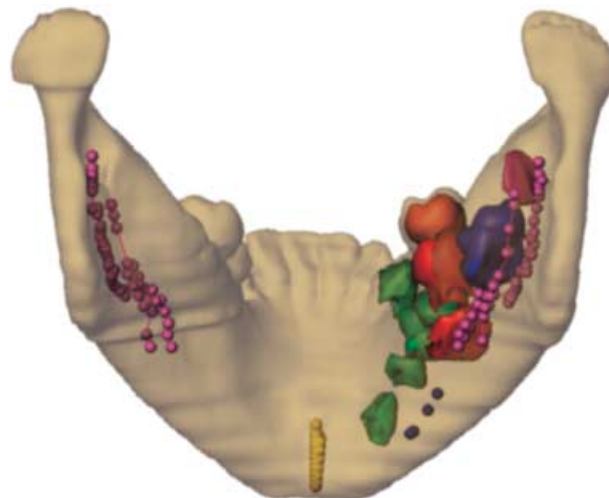


Fig. 12 Patient no. 2. Posterior view. For colour coding see Fig. 10.

Discussion

The purpose of the present study was to analyse normal mandibular growth and tooth eruption in three dimensions, extending the principles of mandibular superimposition on 'stable natural anatomical reference structures' (Björk, 1969; Björk & Skieller, 1983) from two to three dimensions, thereby testing the paradigm related to the stability of these structures. A few previous studies

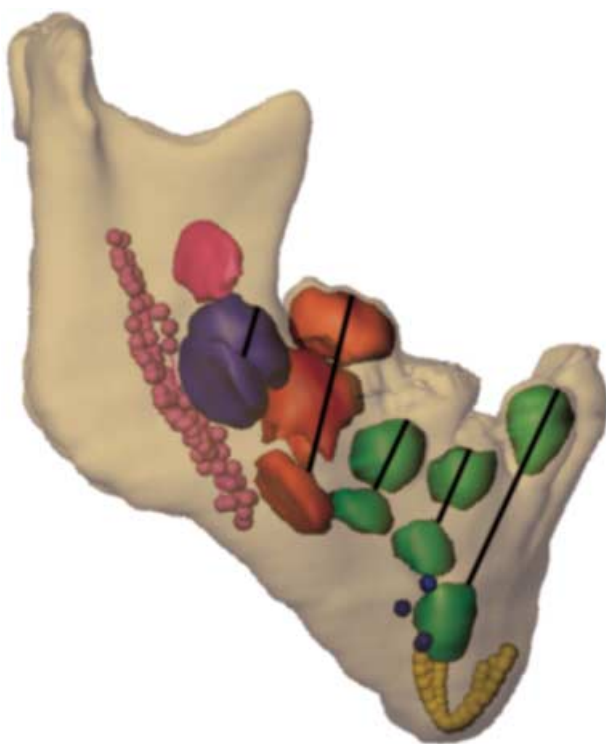


Fig. 13 Patient no. 2. Lateral view. Lines indicate the eruption paths of the individual teeth. For colour coding see Fig. 10.



Fig. 14 Patient no. 2. Oblique view. For colour coding see Fig. 10.

have attempted to analyse mandibular growth in three dimensions. Radlanski et al. (1994, 2003) studied fetal mandibular development cross-sectionally from histological serial sections. Tsai et al. (2004) studied fetal

mandibular development with use of serial 3D sonography. However, no comprehensive study of postnatal mandibular growth and eruption of the permanent teeth has previously been carried out.

Longitudinal craniofacial CT data were available in ten patients with Apert syndrome, and the mandibles from these ten patients were included in the study, as previous reports have documented that the development of the mandible is normal in Apert syndrome (Kreiborg et al. 1999).

Tooth eruption is also fairly normal in the syndrome, although it can be somewhat delayed, but this is primarily true in the hypoplastic maxilla and not in the mandible (Kreiborg & Cohen, 1992; Kaloust et al. 1997). The direction of eruption of the mandibular permanent teeth could, however, be influenced by the narrow, hypoplastic maxilla (Kreiborg et al. 1999), leading to a more lingual direction of tooth eruption than normal.

The error of the landmark digitization determined by duplicate digitizations was found to be within reasonable limits compared with previous findings both in three dimensions (Schleidt, 2002) and in two dimensions (Solow, 1966; Kreiborg, 1981).

The error of the pseudo-landmark digitization was also found to be of an acceptable magnitude, with 80% of the mean differences, d , between the first and the second digitization being below 1 mm, and no errors exceeding 2 mm.

Thus, it can be concluded that both the chosen skeletal and dental landmarks and the pseudo-landmarks can be employed in the analysis of mandibular development and tooth eruption.

By superimposing the longitudinal datasets for each patient on the symphysis menti and the mandibular canals using the automatic method described, mandibular growth was evaluated quantitatively from superimposed computed plots of the symphysis menti and the mandibular canals in the frontal and lateral views of all ten cases.

The results showed that the symphysis menti increased in antero-posterior width, primarily as a consequence of bone apposition posteriorly. This finding is in agreement with the 2D findings of Björk & Skieller (1983). In lateral view, the curvature of the mandibular canals remained relatively stable over time, which was also observed in the 2D studies of Björk (1969) and Björk & Skieller (1983).

However, in the frontal plane, all ten cases showed a lateral shift of the mandibular canals during growth.

This phenomenon has never previously been reported in the literature. This lateral shift could be either the result of a remodelling process or an indication of actual dynamic change in the form of the mandible. The symphysis menti usually fuses during the first year of life (Björk, 1966). However, from birth to 1 year of life a growth in width of the mandible could probably occur at the site of the symphysis menti. Because the first CT scan was obtained prior to 1 year of age in nine of the ten cases, some of the early transverse shift of the mandibular canals could probably be explained by growth in the symphysis menti. However, after the fusion of the symphysis menti the most likely explanation of the lateral shift of the mandibular canals would seem to be bone remodelling with resorption on the buccal side and apposition on the lingual side of the canals. This explanation would seem reasonable given the observed remodelling of the bone surfaces of the mandible showing apposition on the buccal side and resorption on the lingual side. The observed surface remodelling of the mandible in terms of bone apposition at the condyle, coronoid process, alveolar process and posterior aspect of the ramus, and bone resorption at the anterior aspect of the ramus and underneath the gonion is in agreement with previous 2D findings (Björk & Skieller, 1983).

Very few attempts to analyse tooth eruption in three dimensions have previously been made and these studies have been limited to one case (Kreiborg et al. 1996a,b). The findings of the present study were purely qualitative, but they seem to support the hypothesis of Björk (1969) that teeth that have not started forming the root are relatively stable in their position inside the jaw.

Furthermore, the direction of tooth eruption would seem to be vertical for premolars and canines, whereas the mandibular molars seem to have a lingually inclined eruption path. This finding is probably related to the inclination of the teeth inside the jaw, but in the present sample the lingual eruption path could have been influenced by the hypoplastic and narrow maxilla characteristic of subjects with Apert syndrome, as mentioned above (Kreiborg et al. 1999).

In conclusion, the present study would seem to support the paradigm of stability of the symphysis menti and the mandibular canals as seen in profile view. However, the study showed, for the first time, that the mandibular canals are actually relocated laterally during growth, probably primarily due to bone remodelling.

Further research within this field is needed, using 3D techniques, and the methods that we have developed and validated in this study should be used in future studies.

References

- Abbott AH, Netherway DJ, David DJ, Brown T (1990) Application and comparison of techniques for three dimensional analysis of craniofacial anomalies. *J Craniofac Surg* **1**, 119–134.
- Abbott AH, Netherway DJ, Niemann DB, et al. (2000) CT-determined intracranial volume for a normal population. *J Craniofac Surg* **11**, 211–223.
- AnalyzeDirect (1999) Analyze, Version 3.1. ©1999–2001 AnalyzeDirect and ©1986–2001 Mayo Foundation for Medical Education and Research.
- Anamedic. (1999) Mvox, Version 1.41. ©1999 Anamedic & Morten Bro-Nielsen.
- Andresen PR, Bookstein FL, Conradsen K, Ersbøll BK, Marsh JL, Kreiborg S (2000) Surface-bounded growth modelling applied to human mandibles. *IEEE Trans Med Imaging* **19**, 1053–1063.
- Björk A (1951) Some biological aspects of prognathism and occlusion of the teeth. *Angle Orthod* **21**, 3–21.
- Björk A (1955) Facial growth in man, studied with the aid of metallic implants. *Acta Odontol Scand* **13**, 9–34.
- Björk A (1966) Käkarnas tillväxt och utveckling i relation till kraniet i dess helhet. In *Nordisk Klinisk Odontologi I–V*, I, 1 (eds Holst JJ, Østby BN, Osvald O), pp. 1–44. Copenhagen: Forlaget for Faglitteratur.
- Björk A (1968) The use of metallic implants in the study of facial growth in children: method and application. *Am J Phys Anthropol* **29**, 243–254.
- Björk A, Kuroda T (1968) Congenital bilateral hypoplasia of the mandibular condyles associated with congenital bilateral palpebral ptosis. *Am J Orthod* **54**, 584–600.
- Björk A (1969) Prediction of mandibular growth rotation. *Am J Orthod* **55**, 585–599.
- Björk A, Skieller V (1972) Facial growth and tooth eruption. An implant study at the age of puberty. *Am J Orthod* **62**, 339–383.
- Björk A, Skieller V (1983) Normal and abnormal growth of the mandible. A synthesis of longitudinal cephalometric implant studies over a period of 25 years. *Eur J Orthod* **5**, 1–46.
- Broadbent BH (1931) A new x-ray technique and its application to orthodontia. *Angle Orthod* **1**, 45–66.
- Bro-Nielsen M, Larsen P, Kreiborg S (1996) Virtual teeth: a 3D method for editing and visualizing small structures in CT scans. In *Computer Assisted Radiology* (eds Lemke HU, Vannier MW, Inamura K, Farman AG), pp. 921–924. Amsterdam: Elsevier.
- Bro-Nielsen M, Gramkow C, Kreiborg S (1997) Non-rigid registration using bone growth model. In *Lecture Notes in Computer Science 1205* (eds Troccaz J, Grimson E, Mösges R), pp. 3–12. Berlin: Springer.
- Carlsen O (1987) *Dental Morphology*. Copenhagen: Munksgaard.
- Cavalcanti MG, Vannier MW (1998) Quantitative analysis of spiral computed tomography for craniofacial clinical applications. *Dentomaxillofac Radiol* **27**, 344–350.

- Cohen MM Jr** (2000) Apert syndrome. In *Craniosynostosis. Diagnosis, Evaluation, and Management* (eds Cohen M Jr, MacLean R), pp. 316–353. New York: Oxford University Press.
- Dahlberg G** (1940) *Statistical Methods for Medical and Biological Students*. New York: Interscience Publications.
- Dryden IL, Mardia KV** (1998) *Statistical Shape Analysis*. Chichester: John Wiley & Sons.
- Hermann NV, Jensen BL, Dahl E, Darvann TA, Kreiborg S** (2001) A method for three projection infant cephalometry. *Cleft Palate Craniofac J* **38**, 300–316.
- Hilger KB, Larsen P, Kreiborg S, Darvann TA, Marsh JL** (2003) Active shape analysis of mandibular growth. In *Medical Image Computing and Computer-Assisted Intervention (MICCAI) 2003* (eds Ellis RE, Peters TM), pp. 902–909. Berlin: Springer Uerlag.
- Hofrath H** (1931) Die Bedeutung der Röntgenfern- und Abstandsaufnahme für die Diagnostik der Kieferanomalien. *Fortschr Orthod* **1**, 232–258.
- Houston WJB** (1983) The analysis of errors in orthodontic measurements. *Am J Orthod* **83**, 382–390.
- IDL Research Systems** (1997) *Interactive Data Language*, Version 5.0. Boulder, CO: IDL Research Systems.
- Kaloust S, Ishii K, Vargervik K** (1997) Dental development in Apert syndrome. *Cleft Palate Craniofac J* **34**, 117–121.
- Kane AA, Kim YO, Eaton A, Pilgram TK, Marsh JL, Zonneveld F** (2000) Quantification of osseous facial dysmorphology in untreated unilateral coronal synostosis. *Plast Reconstr Surg* **106**, 251–258.
- Kreiborg S, Dahl E, Prydsoe U** (1977) A unit for infant roentgenccephalometry. *Dentomaxillofac Radiol* **6**, 107–111.
- Kreiborg S** (1981) Crouzon syndrome. A clinical and roentgenccephalometric study. *Scand J Plast Reconstr Surg* (Suppl. 18), 1–198.
- Kreiborg S** (1985) The application of roentgenccephalometry to the study of craniofacial anomalies. *J Craniofac Genet Dev Biol Suppl* **1** (1), 31–41.
- Kreiborg S, Cohen MM Jr** (1992) The oral manifestations of Apert syndrome. *J Craniofac Genet Dev Biol* **12**, 41–48.
- Kreiborg S, Marsh JL, Cohen MM Jr, Liversage M, Pedersen H, Skovby F** (1993) Comparative three-dimensional analysis of CT-scans of the calvaria and cranial base in Apert and Crouzon syndromes. *J Cranio-Max-Fac Surg* **21**, 181–188.
- Kreiborg S, Bro-Nielsen M, Larsen P, Darvann T, Dirksen K-L, Skovby F** (1996a) En ny metode til tredimensional analyse af tanddannelse og -eruption. *Tandlægebladet* **100**, 57–58.
- Kreiborg S, Larsen P, Bro-Nielsen M, Darvann T** (1996b) A 3-dimensional analysis of tooth formation and eruption in a case of Apert syndrome. In *Computer Assisted Radiology* (eds Lemke HU, Vannier MW, Inamura K, Farman AG), pp. 1066–1068. Amsterdam: Elsevier.
- Kreiborg S, Aduss H, Cohen MM Jr** (1999) Cephalometric study of the Apert syndrome in adolescence and adulthood. *J Craniofac Genet Dev Biol* **19**, 1–11.
- Kreiborg S, Larsen P, Schleidt DT, Darvann TA, Hermann NV, Dobrzeniecki AB** (2001) New technologies for assessment of craniofacial growth. In *Orthodontics at the Turn of the Century* (eds Kuijpers-Jagtman A-M, Leunisse M), pp. 181–188. Nijmegen: Nederlandse Vereniging voor Orthodontische Studie.
- Lo LJ, Marsh JL, Kane AA, Vannier MW** (1996) Orbital dysmorphology in unilateral coronal synostosis. *Cleft Palate Craniofac J* **33**, 190–197.
- Marsh JL, Vannier MW** (1983) Surface imaging from computerized tomographic scans. *Surgery* **94**, 159–165.
- Marsh JL, Galic M, Vannier MW** (1991) The craniofacial anatomy of Apert syndrome. *Clin Plast Surg* **18**, 237–249.
- Press WH, Teukolsky SA, Vetterling WT, Flannery BP** (1992) *Numerical Recipes in C: the Art of Scientific Computing*, 2nd edn. New York: Cambridge University Press.
- Pruzansky S, Lis EF** (1958) Cephalometric roentgenography of infants: sedation, instrumentation, and research. *Am J Orthod* **44**, 159–186.
- Radlanski RJ, Kjaer I, Vastardis H, Renz H** (1994) Morphometric studies on the fetal development of the human mandible. *Fortschr Kieferorthop* **55**, 77–83.
- Radlanski RJ, Renz H, Klarkowski MC** (2003) Prenatal development of the human mandible. 3D reconstructions, morphometry and bone remodelling pattern, sizes 12–117 mm CRL. *Anat Embryol* **207**, 221–232.
- Ricketts RM** (1981) Perspectives in the clinical application of cephalometrics. *Angle Orthod* **51**, 115–150.
- Schleidt DT** (2002) *Validation of three-dimensional craniofacial imaging of computed tomography*. Thesis. University of Copenhagen.
- Solow B** (1966) The pattern of craniofacial association. A morphological and methodological correlation and factor analysis study on young male adults. *Acta Odontol Scand* **24** (Suppl. 46), 1–174.
- Solow B, Kreiborg S** (1988) A cephalometric unit for research and hospital environments. *Eur J Orthod* **10**, 346–352.
- Tsai M-Y, Lan K-C, Ou C-Y, Chen J-H, Chang S-Y, Hsu T-Y** (2004) Assessment of the facial features and chin development of fetuses with use of serial three-dimensional sonography and the mandibular size monogram in a Chinese population. *Am J Obst Gyn* **190**, 541–546.
- Vannier MW, Pilgram TK, Marsh JL, Kraemer BB, Rayne SC, Gado MH** (1994) Craniosynostosis: diagnostic imaging with three-dimensional CT presentation. *Am J Neurorad* **15**, 1861–1869.
- Vannier MW, Marsh JL** (1996) Three-dimensional imaging, surgical planning, and image-guided surgery. *Radiol Clin North Am* **34**, 545–563.
- Walker GF** (1967) Summary of research report on the analysis of craniofacial growth. *N Zealand Dent J* **63**, 31–38.
- Zhang Z** (1994) Iterative point matching for registration of freeform curves and surfaces. *Int J Computer Vision* **13**, 119–152.
- Zumpano MP, Carson BS, Marsh JL, Vanderkolk CA, Richtsmeier JT** (1999) Three-dimensional morphological analysis of isolated metopic synostosis. *Anat Rec* **256**, 177–188.